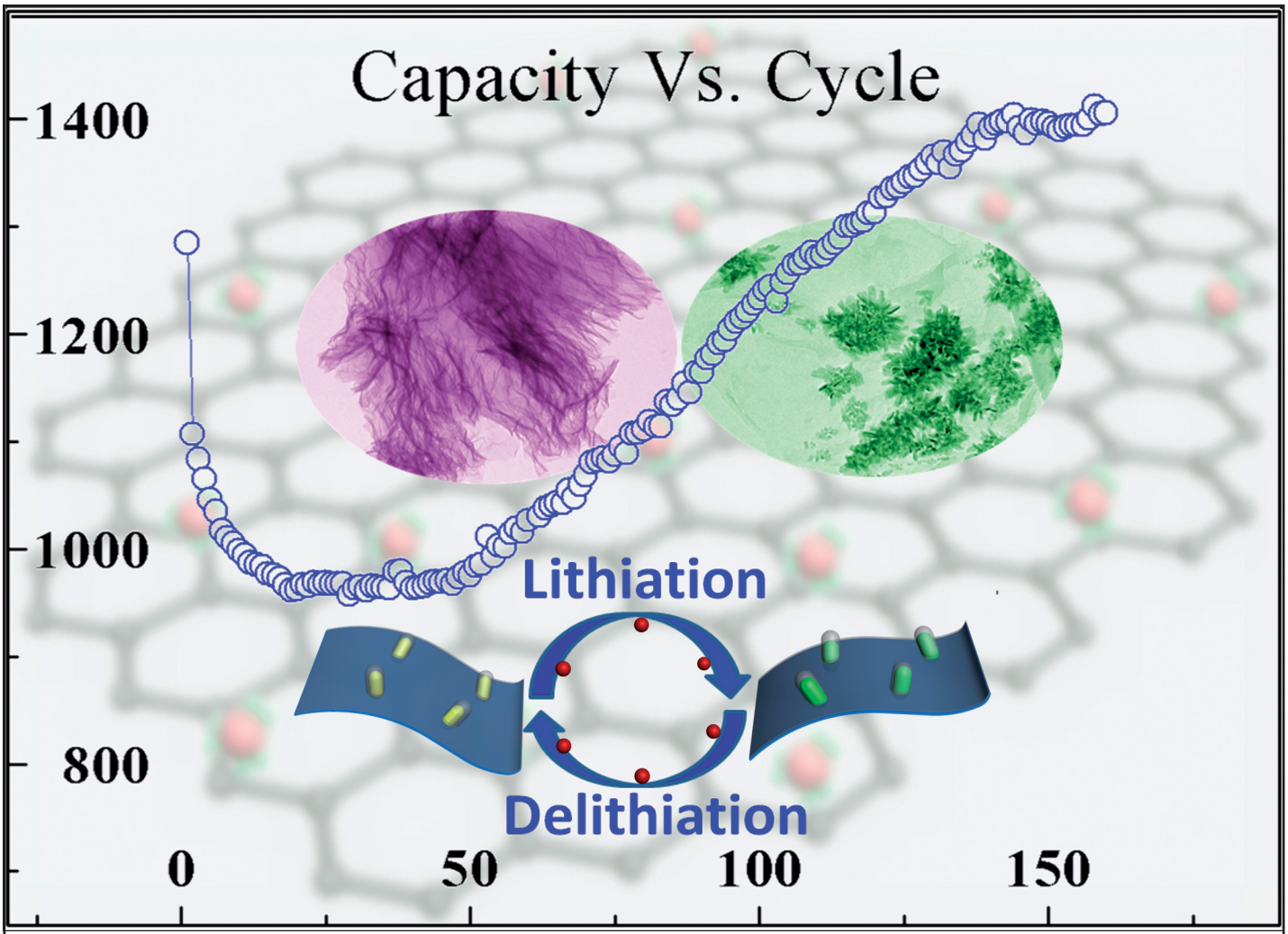

Showcasing research from Dr. Xueliang (Andy) Sun's Nanomaterials and Energy Group (http://www.eng.uwo.ca/people/asun/default.htm) and Dr. Tsun-Kong Sham's Synchrotron Group (http://tsham.chem.uwo.ca/index.html) at Western University, Canada.

Title: Layer by layer assembly of sandwiched graphene/SnO_2 nanorod/carbon nanostructures with ultrahigh lithium ion storage properties

Sandwiched graphene/SnO_2 nanorod/carbon nanostructure is well assembled with strong chemical bonding between layers, indicated by synchrotron analysis. The hybrid electrode exhibits a drastically increased capacity up to 1419 mA h g^{-1} as shown in the image, benefiting from an advanced hierarchical nanostructure.

As featured in:

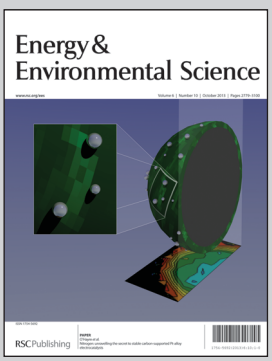

See Sham, Sun *et al.*, *Energy Environ. Sci.*, 2013, **6**, 2900.

RSC Publishing

www.rsc.org/ees

Registered Charity Number 207890

Energy & Environmental Science

RSC Publishing

COMMUNICATION

View Article Online
View Journal | View Issue

Layer by layer assembly of sandwiched graphene/SnO_2 nanorod/carbon nanostructures with ultrahigh lithium ion storage properties†

Cite this: *Energy Environ. Sci.*, 2013, **6**, 2900

Received 9th March 2013
Accepted 28th May 2013

DOI: 10.1039/c3ee40829a

www.rsc.org/ees

Dongniu Wang,[ab] Jinli Yang,[a] Xifei Li,[a] Dongsheng Geng,[a] Ruying Li,[a] Mei Cai,[c] Tsun-Kong Sham*[b] and Xueliang Sun*[a]

Sandwiched structures consisting of carbon coated SnO_2 nanorod grafted on graphene have been synthesized based on a seed assisted hydrothermal growth to form graphene supported SnO_2 nanorods, followed by a nanocarbon coating. As a potential anode for high power and energy applications, the hierarchical nanostructures exhibit a greatly enhanced synergic effect with an extremely high lithium storage capability of up to 1419 mA h g^{-1} benefiting from the advanced structural features.

Broader context

High power/energy density lithium-ion batteries (LIBs) are regarded as a promising energy system for widespread application of electric vehicles and hybrid electric vehicles, which have a large amount of market value in facing the environmental pollution and the depletion of fossil fuels. Exploiting high performance and safe electrodes is crucial for acceleration of the practical use since current graphite based anodes are approaching the limit and they could not satisfy the urgent demand. In this communication, we designed a novel sandwiched hierarchical structure composed of a graphene substrate, intermediate SnO_2 nanorod arrays and the outermost carbon layer. Based on the advantages of the intrinsic structure and the strong chemical bonding between each layers, the sandwiched hybrids exhibit ultrahigh lithium storage as well as excellent rate performances when evaluated as an anode material for LIBs.

Among various energy storage devices, lithium ion batteries (LIBs) have been intensively studied in recent years in connection with the continuously surging market demand for electric vehicles in terms of their high energy density, friendliness to the environment and acceptable high power density.[1–3] In order to store and transport energy more efficiently, a great deal of effort has been made on seeking and developing high performance LIBs, which mainly focuses on choice of electrodes and design of materials' structure. Tin based anodes are regarded as attractive candidates considering their low charge–discharge potentials and high theoretical capacities,[4,5] for example, SnO_2 has a specific capacity of about 780 mA h g^{-1},[6] which is more than twice that of commercialized graphite. However, similar to other high capacity anodes such as silicon[7,8] and germanium,[9,10] the large volume changes (359%) between the fully alloyed and dealloyed states lead to pulverization and severe destruction of the electrode, resulting in fast fading of the capacity.

So far, two main mitigation strategies have been applied; one way is to exploit the structure-dependent properties of SnO_2 anodes.[11] Intensive studies have been carried out and a series of versatile SnO_2 nanostructures, such as nanoparticles,[12,13] nanowires,[5] nanotubes,[14] hollow nanospheres,[6,15] and nanocubes,[16,17] are found to be more sustainable to huge volume change during cycling. However, large-scale productions are hampered both by costly templates[13,18] or surfactants[17] and the requirement of retooling the current equipment. More importantly, the destruction of the desirable morphologies for electrodes could not be truly avoided especially at long cycles and high rates.

Another approach is to focus on fabricating hybrid nanostructures by embedding active Sn based materials into or immobilizing them onto a soft and conductive matrix.[19–24] The highly flexible matrix could buffer the large volume expansion and contraction during cycling to keep the integrity of the whole electrodes intact. Recently, graphene based materials have received enormous attention due to their intriguing and desirable features such as large surface area (>2630 m^2 g^{-1}), excellent electronic conductivity, superior mechanical flexibility, and

[a]*Department of Mechanical and Materials Engineering, University of Western Ontario, London, Ontario, N6A 5B9 Canada. E-mail: xsun@eng.uwo.ca; Tel: +1 519 661-2111 ext. 87759*

[b]*Department of Chemistry, University of Western Ontario, London, Ontario, N6A 5B7 Canada. E-mail: tsham@uwo.ca; Tel: +1 519 661-2111 ext. 86341*

[c]*General Motors R&D Center, Warren, 48090-9055, MI, USA*

† Electronic supplementary information (ESI) available: Experimental part, XPS data of graphene oxide and graphene, elemental mapping spectra and EDX patterns of G/SnO_2 NR/C composites, Raman spectra, TGA curves and coulombic efficiency of G/SnO_2 NR and G/SnO_2 NR/C composites. Differential capacity *versus* voltage plots of G/SnO_2 NR/C composites at selected cycle numbers. Sn M edge spectra of pure Sn, SnO_2 samples and nanocomposites after cycling. See DOI: 10.1039/c3ee40829a

high theoretical capacity (744 mA h g^{-1}).[25,26] In our group, graphene-based electrodes have been widely used in Li ion batteries and Li-air batteries.[27] It is also believed that they will function as an appealing host to homogeneously anchor preferred target materials through their oxygen functionalized groups such as carbonyl (C═O) and carboxylic (C–OOH) bonds.[27a,28] Lots of high performance electrode materials have been realized thorough combining active materials with graphene including Fe_3O_4/graphene,[29] Co_3O_4/graphene,[30] Ge/graphene,[31] and Si/graphene.[32]

Recently, the idea of designing hierarchical nanostructures for LIBs has been implemented by several groups and has led to superior electrochemical performance.[27a,33–37] Interestingly, in these hierarchical nanostructures, experimental capacity higher than theoretical capacity calculated according to a sum of contribution from each component is usually obtained and such a phenomenon is often attributed to the enhanced synergetic effect benefiting from the unique hierarchical nanostructure. Recent results have proved the success and wide adaptability of this concept among various material systems including SnO_2 nanoparticles[33] or SnO_2 nanosheets[34] on graphene, SnO_2@C core–shell structures[35] or hierarchical Sn@C nanoparticles[36] on graphene, carbon coated SnO_2 nanoparticles on CNTs[37] or graphene,[38] multilayered Sn-nanopillar arrays on graphene,[39] and carbon-coated a-Fe_2O_3 hollow nanohorns on the CNT backbone with excellent electrochemical performances.[40]

In this paper, we report a sandwiched hierarchical nanostructure composed of carbon coated SnO_2 nanorods grafted onto the two dimensional (2D) surface of graphene (G/SnO_2 NR/C) based on the above-mentioned idea. Starting from SnO_2 nanoparticle/graphene (G/SnO_2 NP) composites obtained *via* a microwave-assisted hydrothermal method, followed by seed-assisted tin oxide nanorod growth on graphene and subsequent carbon layer coating on top, the layer by layer assembled sandwiched G/SnO_2 NR/C nanocomposites were synthesized for the first time to the best of our knowledge. The 2D graphene network combined with the outermost carbon layer could provide protection to cushion the strain of the SnO_2 nanorod interlayer, which prevents the electrical isolation of SnO_2 nanorods during cycling. Meanwhile, due to the high electronic conductivity of graphene and outer carbon layer, the large surface area and nanoscale diffusion length, high rate capability is expected. As revealed by electrochemical evaluation, it displays ultrahigh lithium storage properties (1419 mA h g^{-1} at the 150th cycle) and a fast lithium insertion–deinsertion process (540 mA h g^{-1} at 3 C).

Graphene was prepared by a modified Hummer's method[27,41,42] and G/SnO_2 NP composites were synthesized by a previously reported microwave-assisted hydrothermal method.[27a] For the synthesis of G/SnO_2 NR composites, the as-obtained G/SnO_2 NP composites were added into an aqueous solution of stannate in a Teflon vessel and then kept at 200 °C for 2 h. It is worth mentioning that the on-top tiny SnO_2 nanoparticles (~3.5 nm) could act as seeds to facilitate the one dimensional growth and the formation of SnO_2 nanorods grafted onto graphene, as demonstrated in Scheme 1. G/SnO_2 NR/C composites were obtained by coating G/SnO_2 NR composites with glucose derived carbon *via* a hydrothermal and continuously sintering process. Detailed procedures can be found in the ESI.†

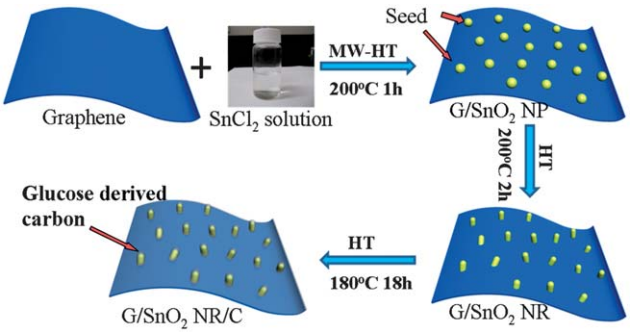

Scheme 1 Illustration of the synthesis processes of G/SnO_2 NR/C nanocomposites: firstly, *in situ* hydrolysis of Sn salts and immobilization of SnO_2 nanoparticles on graphene; secondly, the SnO_2 nanoparticles' seed-assisted hydrothermal process to get SnO_2 NRs grafted onto graphene; finally, nanocarbon coating on G/SnO_2 NR hierarchical structures by hydrothermal carbonization of glucose.

The morphologies and crystallographic structures of the hierarchical G/SnO_2 NR and G/SnO_2 NR/C nanocomposites were determined by electron microscopy images and powder X-ray diffraction (XRD), as shown in Fig. 1. X-ray photoelectron

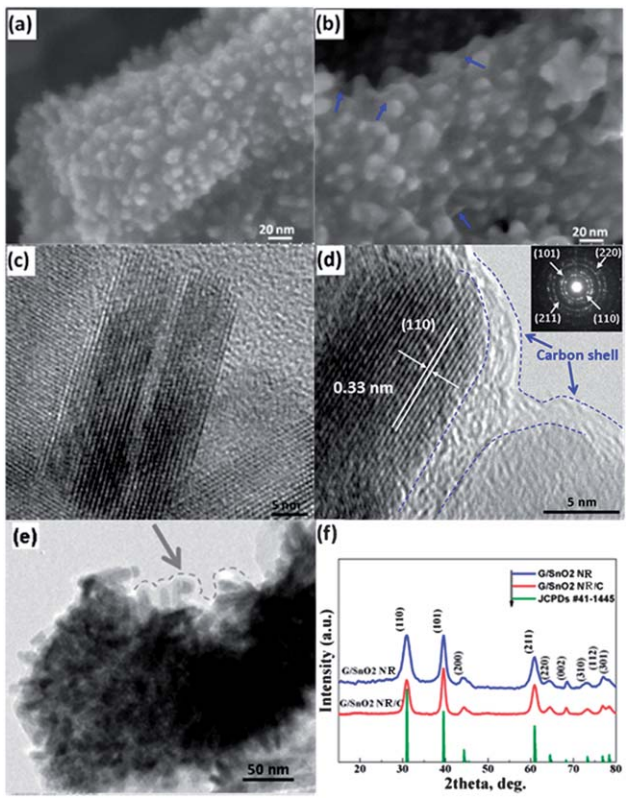

Fig. 1 SEM image of G/SnO_2 NR nanocomposites (a) shows high density of SnO_2 NRs on graphene and the HRTEM image of G/SnO_2 NR hybrids (c) shows no obvious carbon layer; (b) SEM image and (d and e) TEM images of G/SnO_2 NR/C nanocomposites, where arrows indicate the outermost carbon layer; (f) XRD patterns of G/SnO_2 NR and G/SnO_2 NR/C hybrids.

spectroscopy (XPS) data shown in Fig. S1† clearly demonstrate that after thermal reduction, most oxygen groups are removed from graphene oxide to form graphene. The morphologies of pure graphene and G/SnO_2 NP can be found in previous reported results,[27a] where small SnO_2 nanoparticles uniformly deposited on layered graphene. Fig. 1a shows the scanning electron microscopy (SEM) image of G/SnO_2 NR. It can be seen that dense SnO_2 NR arrays become rooted on the entire surface of graphene after hydrothermal treatment of the pre-deposited SnO_2 NPs. It is worth noting that the very small and uniformly distributed SnO_2 NPs[27a] in G/SnO_2 NP composites will function as a "seed" to induce the formation of SnO_2 NRs and confine their growth direction, leading to the homogeneously decorated SnO_2 NR arrays on the 2D graphene surface. The highly crystalline SnO_2 NRs possess a length of around 20–40 nm and a diameter of around 5–7 nm, as shown in Fig. 1c. Fig. 1b, d and e show the morphologies of G/SnO_2 NR/C composites. After nanocarbon coating, the surface of the composites became smoother with an additional ultra thin outermost layer (as arrows pointed), indicating that the carbon layer has been successfully introduced on top of the G/SnO_2 NR hybrids, where SnO_2 NRs are sandwiched between the outermost carbon layer and the graphene substrate to form a sandwiched hierarchical structure. A panoramic view in Fig. 1e reveals that the 2D morphology is still well maintained. The high resolution transmission electron microscopy (HRTEM) image (Fig. 1d) provides further evidence that the SnO_2 NRs are thoroughly covered by carbon with a thickness of 2–3 nm. The inset shows selected area electron diffraction (SAED) patterns representing facets of SnO_2 and a lattice spacing of 3.3 Å which corresponds to the (110) planes of rutile SnO_2, illustrating the high crystallinity of SnO_2 NRs. Moreover, as unveiled by the elemental mapping spectra and energy dispersive X-ray (EDX) patterns of G/SnO_2 NR/C nanocomposites (Fig. S2†), the uniform distributions of C, O, and Sn without other elements confirm the homogeneous distribution of highly purified SnO_2 nanorods in the hybrids.

To gain insight into the internal structure of the composites, XRD experiments were carried out, as shown in Fig. 1f. It can be seen that the XRD patterns for G/SnO_2 NR/C and G/SnO_2 NR composites are quite similar, and all intensive peaks match well with rutile SnO_2 (JCPDS no. 41-1445), illustrating that the crystal structure of SnO_2 remains intact after deposition of the carbon layer. The broadening of the diffraction peaks is consistent with its nanostructure. Raman spectroscopy was further performed to examine the G/SnO_2 NR/C and G/SnO_2 NR composites (Fig. S3a†). The spectrum of graphene (G) was also given for comparison. It is clearly seen that all three samples exhibit intense peaks located at 1340 cm^{-1} and 1582 cm^{-1}, ascribed to the D band and the G band, respectively.[27,43] After deposition of SnO_2 NRs, the intensity ratio of I_D/I_G is almost the same compared with that of pure graphene, indicating that SnO_2 NRs have little effect on the graphitic domains of graphene and the laminated structure remains intact. In contrast, the G/SnO_2 NR/C nanocomposites exhibit both a sharper G band and a higher I_G/I_D value, which should be attributed to the subsequently introduced carbon layer with good graphitic crystallinity. To quantify the contents of SnO_2 NRs and carbon in the composites, thermogravimetric analysis (TGA) was carried out in air with a temperature range from room temperature to 750 °C, as shown in Fig. S3b.† The weight ratio of SnO_2 nanoparticles is calculated as 63.00% for G/SnO_2 NP in our previous report,[27a] after a seed-assisted hydrothermal process to obtain SnO_2 NRs, the weight ratio of SnO_2 increased to 75.64%. With further carbon coating, the weight fraction of carbon in the hybrids increased from 24.36% (100–75.64%) to 31.88% (100–68.12%). All these results, combined with microscope images, demonstrate that hierarchically sandwiched G/SnO_2 NR/C composites have been successfully synthesized.

Desired electrochemical performance of electrodes is highly dependent on the choice of materials and the design of structures. In the sandwiched hierarchical G/SnO_2 NR/C composites, exploiting the electronic structure and chemical information (*e.g.* interaction, bonding and charge transfer) in-between each assembled layer is beneficial for further understanding of the improved electrochemical behavior. To investigate the local chemistry environment of the sandwiched hybrids and more importantly, to reveal the interaction and bonding between layers of the sandwich, X-ray absorption near edge structure spectroscopy (XANES), which is a chemical and elemental sensitive spectroscopic technique, was employed at specific edges of the materials.

Fig. 2a shows the carbon K edge XANES spectra for graphene, G/SnO_2 NP, G/SnO_2 NR and G/SnO_2 NR/C composites. All spectra exhibit two main patterns located at ~285 eV and ~291 eV, which are attributed to graphitic π* and σ* transitions, respectively.[27a,44,45] The existence of these two transitions after deposition of SnO_2 NRs followed by carbon coating indicates that the graphitic framework is kept intact and high electronic conductivity could be expected. Closer observation of the dotted rectangular region (the magnified figure in the inset of Fig. 2a) reveals that the spectra exhibit a gradual shift with some broadening toward the lower energy in the following order: graphene, G/SnO_2 NP, G/SnO_2 NR and G/SnO_2 NR/C hybrids. This observation indicates that after hybridization with SnO_2 nanorods, the carbon 2p-derived π* states in graphene or the outermost carbon layer accept electrons from the n type SnO_2 semiconductor, which is consistent with previously reported results.[27a,44,45] Another noticeable feature is the region between π* and σ* transitions, where the resonances arising are ascribed to the oxygen containing functional groups, namely peak b at 288.2 eV to carbonyl (C═O) and peak c at 289.7 eV to carboxylic (–COOH). Obviously, after SnO_2 NRs are grafted onto graphene, the transition at position c becomes distinct and stronger compared with that of pure graphene and G/SnO_2 NP. The emerging new peak illustrates that SnO_2 NRs are also chemically bonded with surrounding carbon *via* carboxylic in G/SnO_2 NR and G/SnO_2 NR/C composites. The newly established bonding could also be tracked in the case of oxygen K-edge, as shown in Fig. 2b. At position a, the appearance of the shoulder in the G/SnO_2 NR hybrids and much enhanced transition in G/SnO_2 NR/C composites further confirm that SnO_2 NRs are firmly bonded with graphene and the carbon layer through an oxygen functionalized carboxylic group. All these

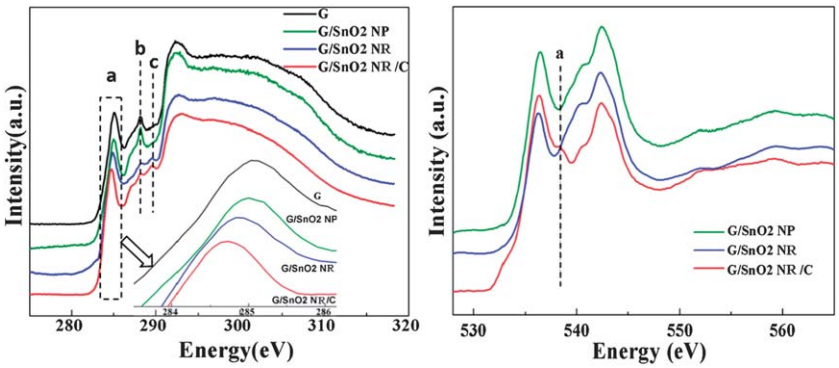

Fig. 2 (a) C K edge XANES spectra of graphene, G/SnO_2 NP, G/SnO_2 NR and G/SnO_2 NR/C composites (the inset is the magnified region which shows a gradual red shift of the π*); (b) O K edge XANES spectra of G/SnO_2 NP, G/SnO_2 NR and G/SnO_2 NR/C composites.

observations, together with the charge transfer behavior at the π* states, provide direct spectroscopic evidence that chemical bonding *via* charge redistribution takes place between the SnO_2 NR layer and the outermost carbon and graphene layers, which anchored the SnO_2 interlayer intimately into a 2D carbon network. Thus, superior electrochemical performance could be expected, benefiting from the hierarchical nanocomposite structure and internal strong chemical bonding.

Intrigued by the structural features of G/SnO_2 NR/C hierarchical structures, we have evaluated their lithium storage properties for potential application as an anode material in LIBs. The charge–discharge profiles at typical cycles of G/SnO_2 NR/C at a current density of 100 mA g^{-1} with a voltage range of 0.01–3 V are shown in Fig. 3a. The hybrids deliver discharge and charge capacities of 1828 mA h g^{-1} and 1285 mA h g^{-1} respectively with an initial coulombic efficiency of 70%. The 30% irreversible capacity loss is attributed to the formation of Li_2O, an inorganic solid electrolyte interface (SEI) film and electrolyte decomposition.[19] From the 10th cycle, the capacity becomes stable and the composites deliver a discharge capacity of 983 mA h g^{-1} up to the 50th cycle. More interestingly, starting from the 50th cycle, the discharge capacity of G/SnO_2 NR/C hierarchical structures increases gradually to 1262 mA h g^{-1} in the 100th cycle and stabilizes at 1419 mA h g^{-1} in the 150th cycle, as shown in the inset of Fig. 3a. To the best of our knowledge, such high electrochemical performance is rarely reported in the literature relating to graphene and other carbon/SnO_2 composites.[19,27a,46] Although behaviors of capacity increase have been reported in SnO_2 and other metal oxide systems, such great capacity increase of almost 440 mA h g^{-1} is not so

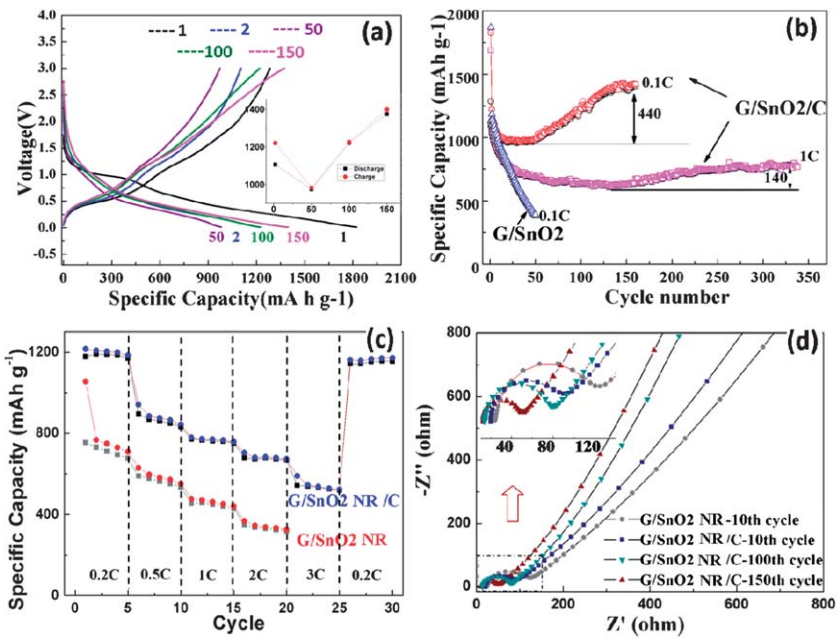

Fig. 3 (a) Charge–discharge profiles of G/SnO_2 NR/C composites (the inset shows the related charge–discharge capacity value *versus* cycle numbers); (b) cycle performance plots of G/SnO_2 NR (0.1 C) and G/SnO_2 NR/C (0.1 C and 1 C) hybrids in the voltage window of 0.01–3.00 V; (c) rate performances of G/SnO_2 NR and G/SnO_2 NR/C nanocomposites; (d) Nyquist plots of G/SnO_2 NR and G/SnO_2 NR/C nanocomposites at specified cycles. Inset: the magnified curves show different diameters of semicircles. Note 1 C = 1000 mA g^{-1}.

common.[19,33,46] Fig. 3b shows the galvanostatic cycle performances of G/SnO_2 NR and G/SnO_2 NR/C nanocomposites. It is found that at the same current density (0.1 C), G/SnO_2 NR nanocomposites exhibit an initial discharge and charge capacity of 1870 and 1133 mA h g^{-1} respectively, with a coulombic efficiency of 60% and continuous decay of the lithium storage capability. At the 50th cycle, it only preserves a discharge capacity of 389 mA h g^{-1}. In contrast, for the G/SnO_2 NR/C sandwiched system, the capacity becomes stable from the 10th cycle with a higher coulombic efficiency of around 98% compared with that of G/SnO_2 NR (Fig. S4†). The inset further confirms the high and stable coulombic efficiency for G/SnO_2 NR/C up to 350 cycles. The higher lithium storage properties and improved coulombic efficiency could only be attributed to the hierarchical sandwiched structure, which thoroughly sealed the SnO_2 NRs inside from the morphological perspective and possessed strong internal chemical bonding between SnO_2 NRs and carbon layer from the spectroscopic perspective. The intact and robust protection could prevent the interlayer SnO_2 NRs from dropping off from the 2D networks during cycling, leading to improved cycling performance. Meanwhile, the outermost carbon layer could inhibit the direct contact between SnO_2 NRs and electrolyte to reduce the amount of irreversible SEI, leading to high coulombic efficiency. More strikingly, the hierarchical structure could offer a dramatically synergic effect and induce a continuous increase of capacity after 50 cycles. Similar capacity boosting is also observed for electrodes cycled at a higher current density of 1 C (1000 mA g^{-1}). As shown in Fig. 3b, the discharge capacity of G/SnO_2 NR/C composites increases from the 100th cycle and stabilized at around 330th cycle with an increment value of 140 mA h g^{-1}, demonstrating that the results are convincing and the electrode has a long cycle life.

Although the reasons for the capacity increase upon cycling are still unclear, the plausible explanations are generally ascribed to the following: as shown in the charge–discharge profiles, by comparing discharge curves in the 100th and 150th cycles with that in the 50th cycle, it is found that part of contribution for capacity increase happens at low voltage (below 0.5 V). Lou and Maier *et al.* attributed such behavior to the reversible formation and decomposition of an organic polymeric/gel like film from the electrolyte, which could provide interfacial storage for excess lithium ions through a so-called "pseudo-capacitance-type behavior".[40,47,48] It is reported that the contact area between the anodes and the electrolyte will also increase due to the inevitable pulverization of SnO_2 along with increasing cycles,[18] resulting in a continuously formed film which provides extra lithium interfacial storage sites as demonstrated in different potential regions.[40,47,48] However, since the contribution of capacity increase from the reversible film is usually limited in a Sn based system, there should be other reasons accounting for high capacity increase (around 440 mA h g^{-1}). On the other hand, Lian *et al.*[33] and Yu *et al.*[49] claimed that such a capacity increase is because the commonly regarded initial irreversible conversion reaction (eqn (1)) is becoming partially reversible upon cycling.

$$SnO_2 + 4Li^+ + 4e^- \rightarrow Sn + 2LiO_2 \quad (1)$$

To confirm this, the differential capacity *versus* voltage plots of G/SnO_2 NR/C composites in typical cycles are also obtained, as shown in Fig. S5.† The initial cathodic process shows a sharp peak at 0.9 V corresponding to the conversion reaction of SnO_2 to Sn and the formation of Li_2O, while it is almost undetectable in the 2nd cycle, indicating that the irreversible conversion process has been completed. However, the peak reappeared at the 100th and 150th cycles, indicating that the conversion reaction happens again and thus it is at least partially reversible. Moreover, in the anodic process, the gradually increased intensity of the peak around 1.3 V after the 50th cycle further demonstrates the growing decomposition of Li_2O upon cycling,[50] where it is prone to oxidize Sn back to SnO_2 in the charged states.[49]

To check the evolution of morphology and structure of the electrodes after charge and discharge processes, HRTEM was further performed on cycled electrodes, as shown in Fig. 4a–d. For G/SnO_2 NR hybrids, after 50 discharge–charge cycles, it is clearly seen that SnO_2 NRs collapsed and pulverized into small particles after cycling. A large field of bare graphene without deposition of SnO_2 indicates that many exposed SnO_2 NRs have detached from the substrate. Fig. 4b shows a small particle left on the edge of graphene and it has no obvious crystalline feature with a size of around 6 nm. In contrast, after 350 discharge–charge cycles, G/SnO_2 NR/C nanocomposites still

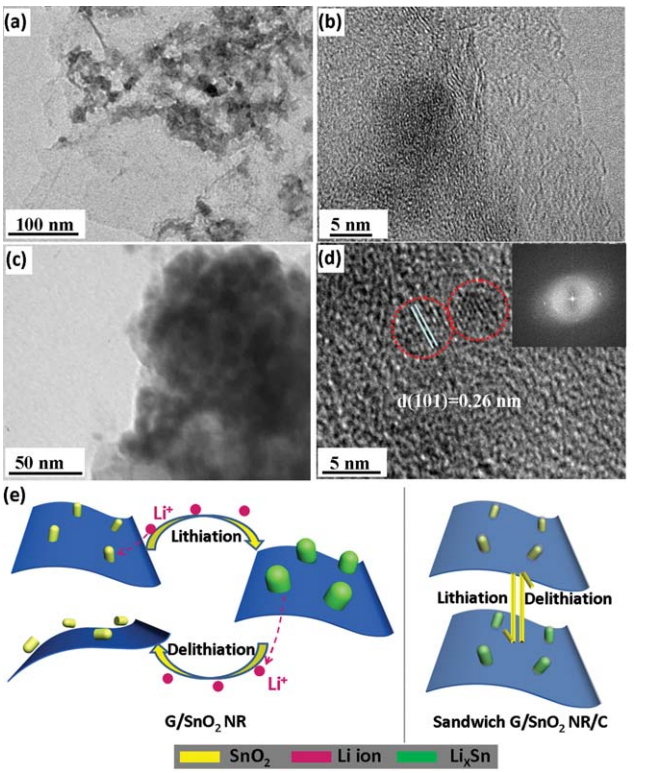

Fig. 4 HRTEM images of nanocomposites after cycling: (a) and (b) G/SnO_2 NR after 50 cycles of discharge–charge at 0.1 C; (c) and (d) G/SnO_2 NR/C after 350 cycles of discharge–charge at 1 C, where the inset shows the Fast Fourier Transform (FFT) electron diffraction pattern taken from the red circled particles; (e) schematic representation showing that the sandwiched structure prevents isolation of SnO_2 NRs during cycling.

maintain their uniform distribution due to the intact protection of the sandwiched hierarchical structure, as shown in Fig. 4c. More importantly, from the high magnification image in Fig. 4d, crystallized nanoparticles with a size of around 2 nm appeared (red circled region). The calculated inter-planar distance is 2.6 Å, which matches well with the (101) facet of SnO_2. The inset Fast Fourier Transform (FFT) electron diffraction pattern taken from the particles further demonstrates their good crystallinity. The direct observation of SnO_2 in cycled electrodes further confirms that the conversion reaction of SnO_2 to Sn and Li_2O is reversible. Also, we performed the XANES at the Sn M edge for the nanocomposites after cycles and compared with pure Sn and SnO_2 standards, as shown in Fig. S6.† It is found that the spectra for cycled G/SnO_2 NR/C nanocomposites and cycled G/SnO_2 NR nanocomposites exhibit distinct difference. Closer observation reveals that the spectrum of cycled G/SnO_2 NR nanocomposites tracks that of pure Sn, while the spectrum of cycled G/SnO_2 NR/C nanocomposites tracks that of pure SnO_2. From the electrochemical curves, the morphologies and the spectra observed here, it is believed that the Sn particles generated from conversion reaction would become small and they are firmly anchored in carbonaceous layers during cycling. With the outermost carbon and graphene protection, Li_2O would be closely surrounded by the smaller and smaller Sn particles. On the other hand, it is well known that the required activation energy for oxidation and solid-state double decomposition reactions would be reduced with the decrease of particle size.[48c] In this case, when the Sn nanoparticles are small enough (*e.g.* 2 nm), the conversion reaction would become reversible as previously predicted by other groups.[33,51,52] It is worth noting that the carbon layer could also prevent the loss of Li_2O from the hierarchical structure upon cycling, favoring its oxidation of Sn to SnO_2.[49] While for G/SnO_2 NR nanocomposites, the exposed Sn and Li_2O would easily detach from graphene during cycling, leading to fast capacity fading. Fig. 4e shows the schematic representation of G/SnO_2 NR and G/SnO_2 NR/C nanocomposites during cycling. Compared with G/SnO_2 NR nanocomposites where the exposed SnO_2 NRs will break away from the graphene substrate and lose their activity, sandwiched G/SnO_2 NR/C nanocomposites exhibit higher cyclability due to the well protection benefiting from the hierarchical structure even at high current density of 1 C.

After 160 discharge–charge cycles at 0.1 C, the same cell for G/SnO_2 NR/C composites is further examined for high power applications, as shown in Fig. 3c. Benefiting from the sandwiched hierarchical structure and robust chemical bonding between layers, the G/SnO_2 NR/C composites display an excellent cycling response from a current density of 0.2 C up to 3 C (3000 mA g^{-1}). Remarkably, a high lithium storage capability of 540 mA h g^{-1} at 3 C could still be obtained for the G/SnO_2 NR/C hybrids. Moreover, a constant capacity of around 1170 mA h g^{-1} can be restored when the current rate was reversed back to 0.2 C. In contrast, a freshly prepared G/SnO_2 NR half cell delivered only 350 mA h g^{-1} at 2 C. Furthermore, AC impedance analysis for the half cell was carried out to elucidate the charge and contact resistance of G/SnO_2 NR and G/SnO_2 NR/C electrodes at selected cycle numbers, as plotted in Fig. 3d. As evident from the drastically smaller diameter of the semicircle for G/SnO_2 NR/C in the 10th cycle compared with that for G/SnO_2 NR, the sandwiched hybrids show much lower impedance than G/SnO_2 NR, benefiting from high conductive carbon coating. Further examinations of the plots at 100th and 150th cycles show even smaller semicircles for G/SnO_2 NR/C (clearly shown in the magnified curves), indicating the increased electron and lithium ion diffusion rate, which results from the irreversible lithiated carbon shells[46] and shortened paths due to the reduced size of Sn nanoparticles upon cycling. Due to the reduced impedance and the facilitated transportation of electrons and lithium ions, G/SnO_2 NR/C composites exhibit both superior cycling and rate performances.

In summary, a sandwiched carbon coated SnO_2 NR grafted on graphene hierarchical structure has been successfully synthesized by a seed assisted hydrothermal growth of SnO_2 nanorods on graphene followed by glucose derived carbon coating. Benefiting from the advanced sandwiched hierarchical structure and the intimate chemical bonding between each layers, the nano-hybrids show drastically increased capacity due to the synergistic effect, which consequently leads to excellent electrochemical performances. The as-prepared G/SnO_2 NR/C nanocomposite exhibits an ultrahigh reversible specific capacity of 1419 mA h g^{-1} in the 150th cycle and high-rate capability at high current densities of 3000 mA g^{-1}. We believe that the synthesis concept could be easily extended to other electrode materials. Our system presented in this work offers significant implications on structural design for improving performances of electrodes in LIBs.

Acknowledgements

This research was supported by Natural Sciences and Engineering Research Council of Canada (NSERC), General Motors of Canada, Canada Research Chair (CRC), Canada Foundation for Innovation (CFI), and Ontario Innovation Trust (OIT) Program. The Canadian Light Source is supported by CFI, NSERC, NRC, CHIR, and the University of Saskatchewan.

References

1 P. G. Bruce, B. Scrosti and J. M. Tarascon, *Angew. Chem., Int. Ed.*, 2008, **47**, 2930–2946.
2 J. M. Tarascon and M. Armand, *Nature*, 2001, **414**, 359–367.
3 Y. Idota, T. Kubota, A. Matsufuji, Y. Maekawa and T. Miyasaka, *Science*, 1997, **276**, 1395–1397.
4 D. Deng and J. Y. Lee, *Angew. Chem., Int. Ed.*, 2009, **48**, 1660–1663.
5 M. S. Park, G. X. Wang, Y. M. Kang, D. Wexler, S. X. Dou and H. K. Liu, *Angew. Chem., Int. Ed.*, 2007, **119**, 764–767.
6 X. W. Lou, C. M. Li and L. A. Archer, *Adv. Mater.*, 2009, **21**, 2536–2539.
7 C. K. Chan, H. L. Peng, G. Liu, K. McIlwrath, X. F. Zhang, R. A. Huggins and Y. Cui, *Nat. Nanotechnol.*, 2008, **3**, 31–35.
8 H. Kim and J. Cho, *Nano Lett.*, 2008, **8**, 3688–3691.
9 M. G. Kim and J. Cho, *J. Electrochem. Soc.*, 2009, **156**, A277–A282.

10 X. L. Wang, W. Q. Han, H. Chen, J. Bai, T. A. Tyson, X. Q. Yu, X. J. Wang and X. Q. Yang, *J. Am. Chem. Soc.*, 2011, **133**, 20692–20695.
11 J. S. Chen and X. W. Lou, *Small*, 2013, **9**, 1877–1893.
12 C. Kim, M. Noh, M. Choi, J. Cho and B. Park, *Chem. Mater.*, 2005, **17**, 3297–3301.
13 H. J. Ahn, H. C. Choi, K. W. Park, S. B. Kim and Y. E. Sung, *J. Phys. Chem. B*, 2004, **108**, 9815–9820.
14 Y. Wang, J. Y. Lee and H. C. Zeng, *Chem. Mater.*, 2005, **17**, 3899–3903.
15 X. W. Lou, L. A. Archer and Z. Yang, *Adv. Mater.*, 2008, **20**, 3987–4019.
16 Z. Wang, D. Luan, F. Boey and X. W. Lou, *J. Am. Chem. Soc.*, 2011, **133**, 4738–4741.
17 R. Liu, S. Yang, F. Wang, X. Lu, Z. Yang and B. Ding, *ACS Appl. Mater. Interfaces*, 2012, **4**, 1537–1542.
18 H. Kim and J. Cho, *J. Mater. Chem.*, 2008, **18**, 771–775.
19 X. Li, X. Meng, J. Liu, D. Geng, Y. Zhang, M. Banis, Y. Li, R. Li, X. Sun, M. Cai and M. Verbrugge, *Adv. Funct. Mater.*, 2012, **22**, 1647–1654.
20 X. Huang, X. Zhou, L. Zhou, K. Qian, Y. Wang, Z. Liu and C. Yu, *ChemPhysChem*, 2011, **12**, 278–281.
21 G. X. Wang, J. H. Ahn, M. J. Lindsay, L. Sun, D. H. Bradhurst, S. X. Dou and H. K. Liu, *J. Power Sources*, 2001, **97**, 211–215.
22 X. Y. Zhao, Z. H. Xia and D. G. Xia, *Electrochim. Acta*, 2010, **55**, 6004–6009.
23 Y. Yu, Q. Yang, D. Teng, X. Yang and S. Ryu, *Electrochem. Commun.*, 2010, **12**, 1187–1190.
24 Y. Wang, H. C. Zeng and J. Y. Lee, *Adv. Mater.*, 2006, **18**, 645–649.
25 S. M. Paek, E. Yoo and I. Honma, *Nano Lett.*, 2009, **9**, 72–75.
26 H. Wang, L. Cui, Y. Yang, H. S. Casalongue, J. T. Robinson, Y. Liang, Y. Cui and H. Dai, *J. Am. Chem. Soc.*, 2010, **132**, 13978–13980.
27 (*a*) D. Wang, X. Li, J. Wang, J. Yang, D. Geng, M. Cai, R. Li, T. K. Sham and X. Sun, *J. Phys. Chem. C*, 2012, **116**, 22149–22156; (*b*) X. Li, D. Geng, Y. Zhang, X. Meng, R. Li and X. Sun, *Electrochem. Commun.*, 2011, **13**, 822–825; (*c*) J. Yang, J. Wang, D. Wang, X. Li, D. Geng, G. Liang, M. Gauthier, R. Li and X. Sun, *J. Power Sources*, 2012, **208**, 340–344; (*d*) J. Yang, J. Wang, Y. Tang, D. Wang, X. Li, Y. Hu, R. Li, G. Liang, T.-K. Sham and X. Sun, *Energy Environ. Sci.*, 2013, **6**, 1521–1528; (*e*) Y. Hu, X. Li, J. Wang, R. Li and X. Sun, *J. Power Sources*, 2013, **237**, 41–46; (*f*) Y. Li, J. Wang, X. Li, D. Geng, R. Li and X. Sun, Superior energy capacity of graphene nanosheets for nonaqueous lithium-oxygen battery, *Chem. Commun.*, 2011, **47**, 9438–9440; (*g*) Y. Li, J. Wang, X. Li, D. Geng, M. Banis, R. Li and X. Sun, *Electrochem. Commun.*, 2012, **18**, 12–15.
28 (*a*) J. Zhou, J. Wang, L. Zuin, T. Regier, Y. Hu, H. Wang, Y. Liang, J. Maley, R. Sammynaiken and H. Dai, *Phys. Chem. Chem. Phys.*, 2012, **14**, 9578–9581; (*b*) J. Zhou, H. Fang, J. M. Maley, J. Y. P. Ko, M. Murphy, Y. Chu, R. Sammynaiken and T. K. Sham, *J. Phys. Chem. C*, 2009, **113**, 6114–6117.
29 G. Zhou, D. W. Wang, F. Li, L. L. Zhang, N. Li, Z. S. Wu, L. Wen, G. Q. Lu and H. M. Cheng, *Chem. Mater.*, 2010, **22**, 5306–5313.
30 S. Q. Chen and Y. Wang, *J. Mater. Chem.*, 2010, **20**, 9735–9739.
31 J. Cheng and J. Du, *CrystEngComm*, 2012, **14**, 397–400.
32 J. K. Lee, K. B. Smith, C. M. Hayner and H. H. Kung, *Chem. Commun.*, 2010, **46**, 2025–2027.
33 P. Lian, X. Zhu, S. Liang, Z. Li, W. Yang and H. Wang, *Electrochim. Acta*, 2011, **56**, 4532–4539.
34 S. Ding, D. Luan, F. Boey, J. S. Chen and X. W. Lou, *Chem. Commun.*, 2011, **47**, 7155–7157.
35 Z. Y. Wang, Z. C. Wang, S. Madhavi and X. W. Lou, *J. Mater. Chem.*, 2012, **22**, 2526–2531.
36 Y. Q. Zou and Y. Wang, *ACS Nano*, 2011, **5**, 8108–8114.
37 S. Ding, J. S. Chen and X. W. Lou, *Chem.–Asian J.*, 2011, **6**, 2278–2281.
38 J. Cheng, H. Xin, H. Zheng and B. Wang, *J. Power Sources*, 2013, **232**, 152–158.
39 L. Ji, Z. Tan, T. Kuykendall, E. J. An, Y. Fu, V. Battaglia and Y. Zhang, *Energy Environ. Sci.*, 2011, **4**, 3611–3616.
40 Z. Wang, D. Luan, S. Madhavi, Y. Hu and X. W. Lou, *Energy Environ. Sci.*, 2012, **5**, 5252–5256.
41 W. S. Hummers and R. E. Offeman, *J. Am. Chem. Soc.*, 1958, **80**, 1339.
42 D. Geng, Y. Chen, Y. Chen, Y. Li, R. Li, X. Sun, S. Ye and S. Knights, *Energy Environ. Sci.*, 2011, **4**, 760–764.
43 F. Tuinstra and J. L. Koenig, *J. Chem. Phys.*, 1970, **53**, 1126–1130.
44 J. Zhou, J. Wang, H. Fang and T. K. Sham, *J. Mater. Chem.*, 2011, **21**, 5944–5949.
45 J. Zhou, J. Wang, H. Fang, C. Wu, J. N. Cutler and T. K. Sham, *Chem. Commun.*, 2010, **46**, 2778–2780.
46 Y. Su, S. Li, D. Wu, F. Zhang, H. Liang, P. Gao, C. Cheng and X. Feng, *ACS Nano*, 2012, **6**, 8349–8356.
47 J. Jamnik and J. Maier, *Phys. Chem. Chem. Phys.*, 2003, **5**, 5215–5220.
48 (*a*) P. Poizot, S. Laruelle, S. Grugeon, L. Dupont and J.-M. Tarascon, *Nature*, 2000, **407**, 496–499; (*b*) S. Laruelle, S. Grugeon, P. Poizot, M. Dollé, L. Dupont and J.-M. Tarascon, *J. Electrochem. Soc.*, 2002, **149**, A627–A634; (*c*) P. L. Taberna, S. Mitra, P. Poizot, P. Simon and J. M. Tarascon, *Nat. Mater.*, 2006, **5**, 567–573.
49 Y. Yu, C. Chen and Y. Shi, *Adv. Mater.*, 2007, **19**, 993–997.
50 I. A. Courtney and J. R. Dahn, *J. Electrochem. Soc.*, 1997, **144**, 2943–2948.
51 R. Demir-Cakan, Y. S. Hu, M. Antonietti, J. Maier and M. M. Titirici, *Chem. Mater.*, 2008, **20**, 1227–1229.
52 S. Han, B. Jang, T. Kim, S. M. Oh and T. Hyeon, *Adv. Funct. Mater.*, 2005, **15**, 1845–1850.

